ADVANCES IN ATMOSPHERIC SCIENCES, VOL. 30, NO. 6, 2013, 1695–1711

A Modeling Analysis of Rainfall and Water Cycle by the Cloud-resolving WRF Model over the Western North Pacific

GAO Wenhua[1,2] (高文华) and SUI Chung-Hsiung*[2] (隋中兴)

[1] *State Key Laboratory of Severe Weather, Chinese Academy of Meteorological Sciences, Beijing* 100081

[2] *Department of Atmospheric Sciences, NTU, Taipei* 10617

(Received 20 November 2012; revised 29 January 2013; accepted 11 March 2013)

ABSTRACT

Simulated regional precipitation, especially extreme precipitation events, and the regional hydrologic budgets over the western North Pacific region during the period from May to June 2008 were investigated with the high-resolution (4-km grid spacing) Weather Research and Forecast (WRF v3.2.1) model with explicit cloud microphysics. The model initial and boundary conditions were derived from the National Centers for Environmental Prediction/Department of Energy (NCEP/DOE) Reanalysis 2 data.

The model precipitation results were evaluated against the Tropical Rainfall Measuring Mission (TRMM) Multisatellite Precipitation Analysis 3B42 product. The results show that the WRF simulations can reasonably reproduce the spatial distributions of daily mean precipitation and rainy days. However, the simulated frequency distributions of rainy days showed an overestimation of light precipitation, an underestimation of moderate to heavy precipitation, but a good representation of extreme precipitation. The downscaling approach was able to add value to the very heavy precipitation over the ocean since the convective processes are resolved by the high-resolution cloud-resolving model. Moreover, the water vapor budget analysis indicates that heavy precipitation is contributed mostly by the stronger moisture convergence; whereas, in less convective periods, the precipitation is more influenced by the surface evaporation. The simulated water vapor budgets imply the importance in the tropical monsoon region of cloud microphysics that affects the precipitation, atmospheric latent heating and, subsequently, the large-scale circulation.

Key words: cloud-resolving, WRF, precipitation, western North Pacific

Citation: Gao, W. H., and C.-H. Sui, 2013: A modeling analysis of rainfall and water cycle by the cloud-resolving WRF model over the western North Pacific. *Adv. Atmos. Sci.*, **30**(6), 1695–1711, doi: 10.1007/s00376-013-2288-8.

1. Introduction

Precipitation is an essential parameter describing the monsoon climate. The spatial distribution of precipitation indicates the location of atmospheric latent heating, and the evolution of precipitation reflects the variability of the monsoon circulation system. Meanwhile, precipitation is also a key component of the Earth's water cycle. Studying precipitation characteristics is very important for understanding monsoon circulation and its relationship with the Earth's water cycle. However, accurate simulation of summer precipitation, particularly in tropical regions, remains a major challenge (Jenkins, 1997; Kunkel et al., 2002). Modeling and predicting tropical atmospheric phenomena such as summer monsoon activity still has its barriers because of a lack of fundamental knowledge about tropical convection interacting with tropical circulation.

The East Asian (EA) monsoon and western North Pacific (WNP) monsoon affect not only the regional climate but also the global climate through water and energy exchange processes (Lau and Weng, 2002). In the past two decades, studies on the WNP summer monsoon by using reanalysis data and satellite precipitation datasets have been conducted (Murakami

*Corresponding author: SUI Chung-Hsiung, sui@as.ntu.edu.tw

and Matsumoto, 1994; Wang et al., 2001; Wang and LinHo, 2002; Conroy and Overpeck, 2011). The climate over the WNP region depends on the atmospheric and oceanic conditions of tropical and subtropical regions. So, moisture transport and the hydrological cycle over the EA–WNP region are more complex than those over other regions. For example, the sources of water vapor variation over the EA–WNP region can come from three areas: the northern Indian Ocean, the South China Sea (SCS), and the WNP (Zhou and Yu, 2005; Ding and Sikka, 2006). Furthermore, the spatial heterogeneity of rainfall in this region may respond nonlinearly to changes in the forcing factors (Zhou et al., 2009). Owing to a lack of conventional observations, relatively few studies to date have been dedicated to regional model performance over the WNP region. Our study focuses on the climatology during the onset of the SCS–WNP summer monsoon in the period from May to June 2008.

It is known that in existing global general circulation models (GCMs), horizontal grid intervals are too coarse for applications at regional-scale regimes (Leung et al., 2003; Giorgi, 2006). To mitigate this problem, a dynamical downscaling strategy to represent regional weather phenomena influenced by the local topography or small-scale atmospheric features has been conducted in many previous studies (Giorgi, 1990; Christensen et al., 1998; Liang et al., 2004; Castro et al., 2005; Kanamitsu and Kanamaru, 2007), in which GCM or reanalysis data are used to provide the boundary conditions for more spatially-detailed climatological simulations over a region of interest. Note that regional models can add value, but only for certain variables and locations. Winterfeldt et al. (2010) showed that dynamical downscaling does not add value to the wind speed in open ocean areas because of the relatively homogeneous surface over the ocean. In addition, the effects of spatial resolution on regional climate simulations have been extensively discussed. Leung and Qian (2003) analyzed the results of 5-yr regional simulations for the Northwest Pacific and California, and demonstrated that a 13-km nest produces more realistic seasonal mean precipitation as well as more frequent heavy precipitation compared to a 40-km nest. Kobayashi and Sugi (2004) showed that synoptic-scale climate phenomena are well represented and more tropical cyclones with higher intensities can be captured when GCM resolution is increased, therefore improving the simulation of Asian monsoon. Improved precipitation simulation with higher spatial resolution has generally been reported in many climate studies due to the detailed representation of terrain effects and spatial heterogeneity, as well as the better depiction of mesoscale processes. But still, most regional climate simulations continue to use a relatively coarse grid resolution (about 10–40 km).

In addition, Randall et al. (2007) pointed out that the cumulus parameterization scheme used in GCMs is another major cause of ambiguity for climate simulation. Details of cloud microphysics are beginning to be introduced into regional climate studies. Miura et al. (2007) conducted a global cloud resolving simulation with a grid size of a few kilometers in a nonhydrostatic icosahedral atmospheric model (NICAM). Tao et al. (2003b) simulated the mesoscale convective systems over the SCS region with a regional climate model and a cloud-resolving model, and indicated that a better reproduction of rainfall processes probably needs cloud-scale models. The impacts of cloud microphysics on simulated surface precipitation have been widely studied (Jankov et al., 2009; Chin et al., 2010). Milbrandt et al. (2010) reported a great sensitivity in both precipitation and hydrometeor mass fields to the number of predicted moments in a bulk microphysics scheme. However, until recently, few models have been run only explicitly using microphysics (i.e., no cumulus parameterization) and with fine enough grid spacing to investigate the regional climate mechanisms.

The long-term goal of this study is to refine our understanding of clouds and precipitation over the tropical Pacific warm pool and their interaction with climate oscillations at seasonal or longer time scales. So, the basic properties of simulated precipitation as well as the regional water cycle within the framework of high-resolution dynamical downscaling should first be explored. Several questions should be addressed in this context: (1) How well does Weather Research and Forecast (WRF) model high-resolution downscaling simulated precipitation agree with observations over the WNP region? (2) Is the microphysics crucial for adequate performance of climatological precipitation over the ocean? (3) How well does the WRF model represent regional hydrologic budgets?

The primary focus of this paper is to report upon investigations into the capability of the cloud-resolving WRF model to simulate the characteristics of regional precipitation, especially extreme precipitation events, as well as regional hydrologic budgets, over the WNP region. The paper is organized as follows. Section 2 describes the model, data and experimental design. Section 3 examines the thermodynamic variables. Section 4 discusses the simulated and observed daily mean precipitation, percentage of rainy days, precipitation frequency distribution and extreme precipitation. The hydrologic budgets are presented in section 5, and a summary is given in section 6.

2. Numerical model and validation dataset

2.1 *Model description and experimental design*

The model employed was the WRF model version 3.2.1 (Skamarock et al., 2008). It is a non-hydrostatic, terrain-following meso-scale model, and is designed for short-term weather forecasting and long-term climate simulation.

The Chinese Academy of Meteorological Sciences (CAMS) two-moment microphysics scheme was adopted as an alternative microphysical scheme. It was developed by Hu and He (1988) and has been tested and employed in many previous studies (Hu and He, 1989; Lou et al., 2003; Li et al., 2008; Gao et al., 2011a, b). A total of 11 microphysical variables including the mixing ratio of vapor, the mixing ratios and number concentrations of cloud droplets, rain, cloud ice, snow, and graupel are predicted in the CAMS microphysics scheme. In recent years, the scheme has been significantly improved, such as a more accurate calculation of supersaturation, more detailed treatment of autoconversion and droplet nucleation parameterization. Gao et al. (2011b) evaluated and improved the CAMS raindrop microphysical parameterization against Southwest Monsoon Experiment (SoWMEX)/Terrain-influenced Monsoon Rainfall Experiment (TiMREX) observations in June 2008.

The model domain is designed to consist of three one-way nested domains, as shown in Fig. 1. The number of grid points (lon×lat×height) and corresponding grid resolutions for domains 1, 2 and 3 are 290×210×35 at 36 km, 541×421×35 at 12 km, and 883×691×35 at 4 km, respectively. To capture the large-scale processes important to the WNP climate, the outermost domain covers the entire East and Central Asia continental area and much of the western Pacific Ocean. Such a large outer domain ensures that the weather systems approaching the WNP region are free from lateral boundary influences. The second nested domain covers the EA continent and the WNP region. The innermost domain covers the SCS and portions of the WNP region.

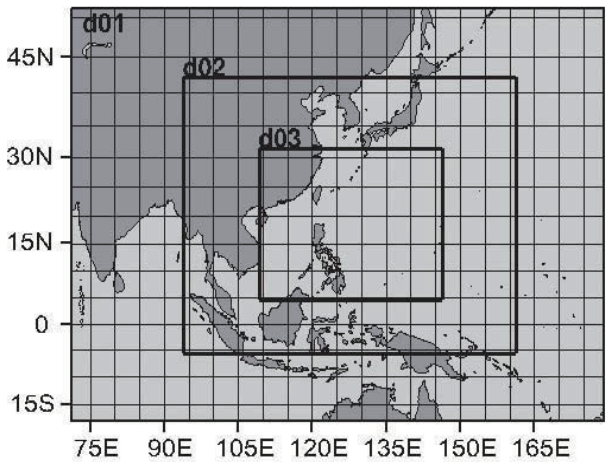

Fig. 1. Geographic locations of the three domains used in the numerical simulation.

For non-hydrostatic cloud resolving models, the grid resolution has certain impact on the resolved convective processes. Weisman et al. (1997) suggested that a minimum grid size of 4 km is required to reasonably simulate the internal structures and meso-scale circulations of a mid-latitude squall line. Satoh et al. (2010) showed using a global cloud-resolving model with mesh sizes of 3.5, 7 and 14 km, along with satellite data, that the simulated cloud thickness and size of mesoscale convective system depend quantitatively on the model resolution. Based on the above considerations and the limitation of computer resources, we chose the grid size of 4 km for the current study.

The initial and lateral boundary conditions were interpolated from the National Centers for Environmental Prediction/Department of Energy (NCEP/DOE) Reanalysis 2 data (hereafter R2) (Kanamitsu et al., 2002). The lateral boundary conditions were updated every six hours. Because the study area is over the ocean, the SST is important to the simulated precipitation (Wu et al., 2009; Hill et al., 2011), so the SST used in the WRF model was also updated every six hours from R2 data. The physics schemes used were the Noah land surface model (Chen and Dudhia, 2001), the Yonsei University (YSU) planetary boundary layer scheme (Hong et al., 2006), the Grell-Devenyi cumulus parameterization scheme (Grell and Devenyi, 2002), the rapid radiative transfer model longwave radiation scheme (Mlawer et al., 1997), and the Dudhia shortwave radiation scheme (Dudhia, 1989). No cumulus parameterization was used in domain 3. In order to assess the impact of microphysics on the precipitation process at a model resolution of 4 km, two cloud microphysics schemes were used: the Goddard 3ICE (Tao and Simpson, 1993) and the CAMS scheme. Goddard 3ICE is a one-moment scheme; it predicts only the mixing ratios for five hydrometeor species. Tao et al. (2003a) later added new saturation techniques in the microphysical processes related to phase change. Whereas, the CAMS microphysics is a two-moment scheme; it predicts both the mixing ratios and number concentrations for five hydrometeor species.

The simulation period was from 0000 UTC 1 May to 2400 UTC 30 June 2008. The model was re-initialized every two days. Each re-initialization ran

for 12 hours proceeding the initial time of each 2-day simulation by nudging the horizontal winds above 850 hPa toward the reanalysis values. The re-initialization was a simple spin-up run to produce a set of initial fields in the two-month integration period to mitigate climate drift in regional climate simulations (Dickinson et al., 1989; Qian et al., 2003). The grid nudging was applied in the two outer model domains but not in the innermost domain, which allowed the model to freely develop atmospheric structure at a finer spatial scale. The model outputs at every 6 hours were used for the evaluation.

2.2 *Validation dataset*

The Tropical Rainfall Measuring Mission (TRMM) 3B42 rainfall product version 6, a high spatial ($0.25° \times 0.25°$) and high temporal (3 h) satellite-derived precipitation dataset available in the latitude band 50°S–50°N from 1 January 1998 to present, was used to validate the simulation results. These data are created by blending passive microwave data [e.g., TRMM Microwave Imager (TMI), Special Sensor Microwave Imager (SSM/I), Advanced Microwave Scanning Radiometer (AMSR), Advanced Microwave Sounding Unit (AMSU)] and infrared (IR) data collected at geosynchronous Earth orbit and based on calibration by the TMI-PR combined rain estimates. The physics-based microwave rain estimates were used where available, and the remaining areas were filled with the IR rain estimates calibrated by microwave data (Huffman et al., 2007).

3. Evaluation of model thermodynamic variables

To evaluate the state variables, we compared the model-simulated temperature and humidity with R2 data. Figure 2 shows the difference of mean dry static energy (DSE $= c_pT + gz$, where c_p is the specific heat at constant pressure, T the absolute temperature, g the gravitational acceleration, and z the height above surface) and latent heat energy ($L_\mathrm{v}q_\mathrm{v}$, where L_v is the latent heat of vaporization, q_v the water vapor mixing ratio) averaged over domain 3 during May and June 2008 between WRF simulations and R2 data. The value of DSE shown in Fig. 2a was determined mainly by the air temperature. The model temperature by the two cloud schemes differed from the R2 data within 1°C, and the CAMS-scheme-simulated temperature was slightly warmer than that in the Goddard scheme. Compared with the R2 data, the two simulations showed a common warm bias in the upper troposphere above 200 hPa, and a common cold bias in the lower troposphere below 850 hPa. Associated

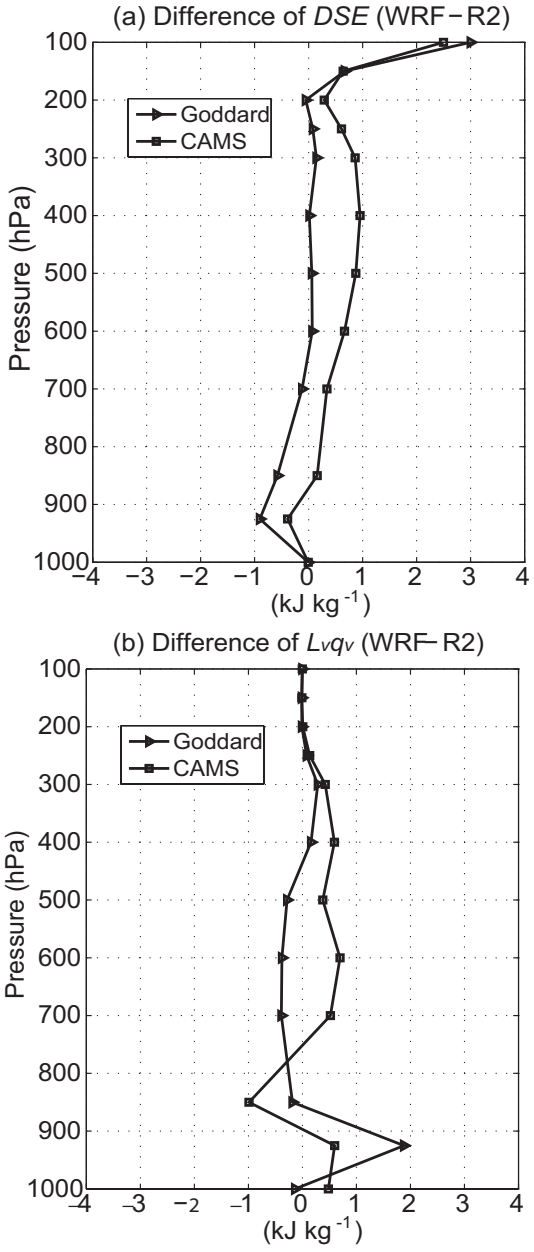

Fig. 2. Difference of (a) DSE and (b) $L_\mathrm{v}q_\mathrm{v}$ (kJ kg^{-1}) between the WRF simulations and R2.

with the model cold bias in the lower troposphere, model results also showed a common moist bias. However, the two microphysics schemes produced opposite moisture biases above 850 hPa. The larger amount of precipitation in the CAMS scheme suggests stronger convective activities and thus greater latent heating, leading to warmer temperatures. Additionally, the stronger convection in the CAMS scheme would result in stronger vertical moisture transport from the PBL to upper levels, responsible for the wetter free troposphere and drier PBL, than those in the God-

dard scheme.

The diurnal cycles of model temperature and humidity were further examined by forming a diurnal composite of the vertically-integrated saturation water vapor mixing ratio (q_s) and the water vapor mixing ratio averaged over domain 3 from 30 consecutive two-day integrations. The composites for q_s and q_v are shown in Fig. 3a and 3b, respectively. Since q_s is a function of temperature, the diurnal q_s from R2 shows a maximum value near 0600 UTC (1400 LST) and a cooling trend toward a minimum value near 2400 UTC (0800 LST) with an amplitude of about 4 kg m^{-2}. The two WRF simulations show a similar diurnal change characterized by a warm phase near 0600 to 1200 UTC and a cold phase near 1800 to 2400 UTC with a smoother phase change and a weaker amplitude than in R2. The difference between the simulated and assimilated q_s probably resulted from the cloud radiative interactions in the cloud-resolving physics. The higher q_s from the CAMS scheme than that from the Goddard scheme (by about 1–3 kg m^{-2}) is consistent with the difference in simulated DSE profiles. The composite curves of q_v for the model and R2 data show weaker diurnal cycles with no consistent phase changes. This indicates that the water vapor field in domain 3 is mainly dominated by synoptic-scale disturbances. The simulated q_v by the CAMS scheme was somewhat larger than that by the Goddard scheme, but the simulated precipitation by the CAMS scheme was significantly larger than that by the Goddard scheme, which correlated with the moisture convergence. This will be discussed in detail in section 5.

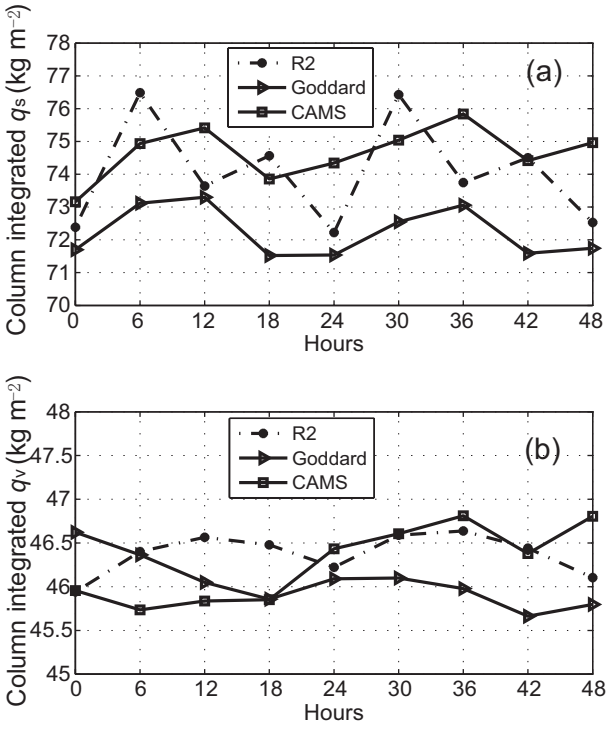

Fig. 3. Diurnal composites of vertically integrated (a) saturation water vapor mixing ratio and (b) water vapor mixing ratio (kg m^{-2}) averaged over domain 3 from 30 consecutive two-day integrations.

4. Evaluation of model precipitation

Precipitation is an important quantity in climate studies, and reducing the precipitation bias is one of the major goals for regional climate simulations. TRMM 3B42 daily precipitation data were used as a reference in this study. The R2 data and WRF simulations were spatially re-gridded onto 0.25° grid points, the same as the TRMM dataset, for point-by-point comparison purposes. Interpolation was not used when calculating the precipitation frequency.

4.1 *Mean precipitation pattern*

Figure 4 shows the spatial distribution of time-mean precipitation during May to June 2008 from TRMM observations, R2 data, and WRF simulations. The major monsoon rainbands were located over the Philippine Sea, SCS, and the southeast China coast. The location of the rainfall center over the ocean was near (9.5°N, 131°E), and the maximum value was about 21 mm d^{-1} (Fig. 4a). The WRF simulations reproduced the characteristics of daily mean precipitation well based on a comparison with TRMM observations. The patterns of spatial distribution from the WRF model showed clear improvement compared with R2, which produced a wet bias over the ocean, and a strong dry bias over the southeast China coast. The Goddard scheme reduced the wet bias of R2 over the ocean, and the CAMS scheme introduced a wet bias relative to R2. Though the CAMS scheme produced the maximum daily mean precipitation with a value of about 21 mm d^{-1} over the ocean, which is similar to the TRMM observation, it overestimated to a certain extent the range of heavy precipitation. The spatial distributions of daily mean precipitation in Fig. 4 show that the two microphysics schemes produced similar precipitation patterns, but quite different precipitation amounts.

To quantitatively evaluate the performances of the WRF model in its simulation of precipitation, the time-mean precipitation averaged over domain 3, the pattern root mean square error (RMSE) and pattern correlation coefficients with respect to TRMM observations are listed in Table 1. The results show that the simulated spatial and temporal mean precipitation in

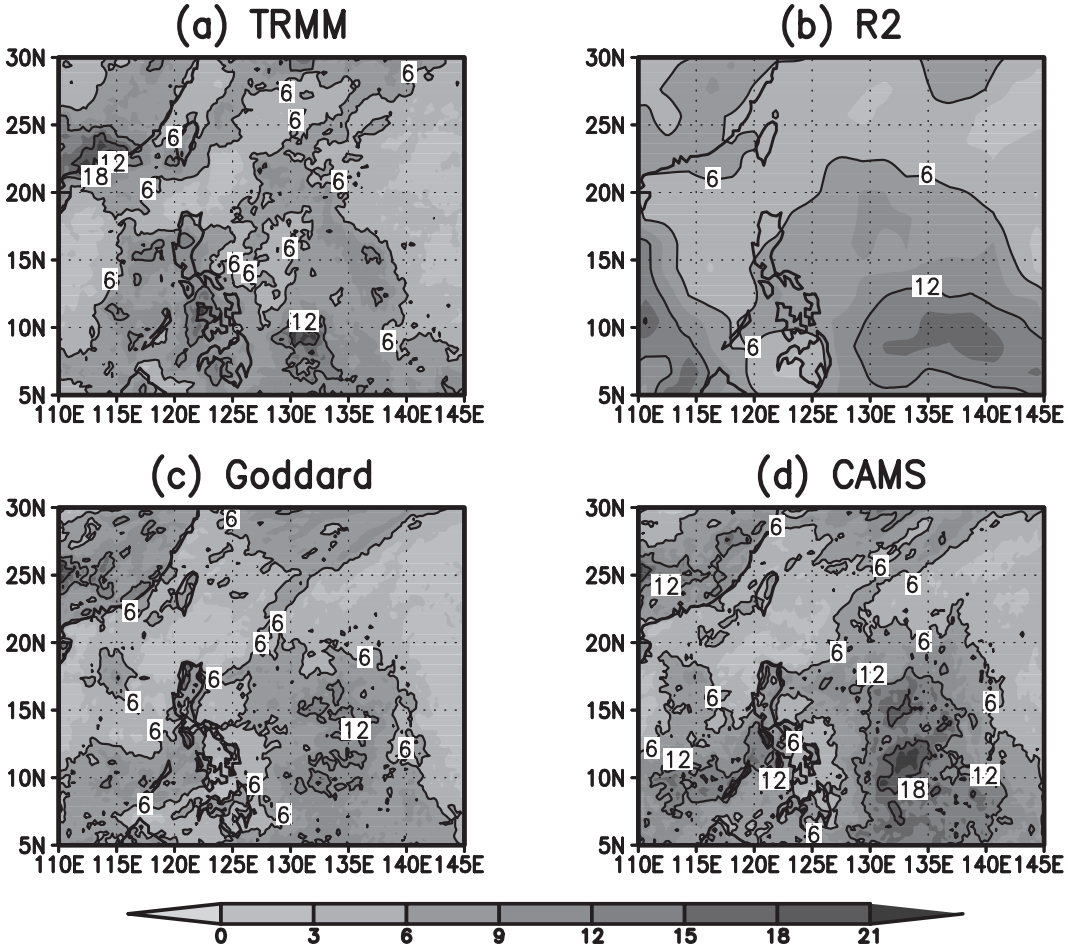

Fig. 4. Spatial distribution of daily mean precipitation (mm d^{-1}) during May to June 2008 from (a) TRMM, (b) R2, and (c, d) WRF simulations.

Table 1. Area-averaged daily mean precipitation (mm d^{-1}), pattern RMSE (mm d^{-1}) and pattern correlation coefficients between the observed and simulated daily mean precipitation shown in Fig. 4.

	Mean	Spatial RMSE	Spatial correlation
TRMM	7.03	–	–
R2	7.38	4.20	0.26
Goddard	6.24	3.26	0.53
CAMS	8.01	4.00	0.48

the Goddard scheme was slightly less than in the observation, while that in the CAMS scheme was somewhat larger, indicating that climatological precipitation in the northwest Pacific warm monsoon season is sensitive to the cloud microphysics scheme. Note that the two-moment microphysics does not necessarily correspond to more accurate precipitation compared to the one-moment microphysics scheme because there are still many uncertainties in the cloud microphysics parameterizations, especially in long-term simulations. Wang et al. (2003) and Lee et al. (2004) also showed that the skill in simulating tropical precipitation systems is generally poorer than that in mid-latitude systems due to weak baroclinic instability and complicated physical processes in East Asia. Table 1 further shows that the precipitation simulated by the two microphysics schemes had smaller pattern RMSE and higher pattern correlation with the TRMM precipitation than that by R2. This indicates that the high-resolution WRF, with an explicit cloud microphysics scheme, can reasonably resolve mesoscale variability, and is capable of simulating the accumulated precipitation distribution in properly designed regional downscaling simulations.

4.2 *Temporal evolution of precipitation*

The model performances in reproducing the northward migration of tropical and subtropical fronts and associated rain bands were examined. Figure 5 shows the time–latitude cross section of daily precipitation

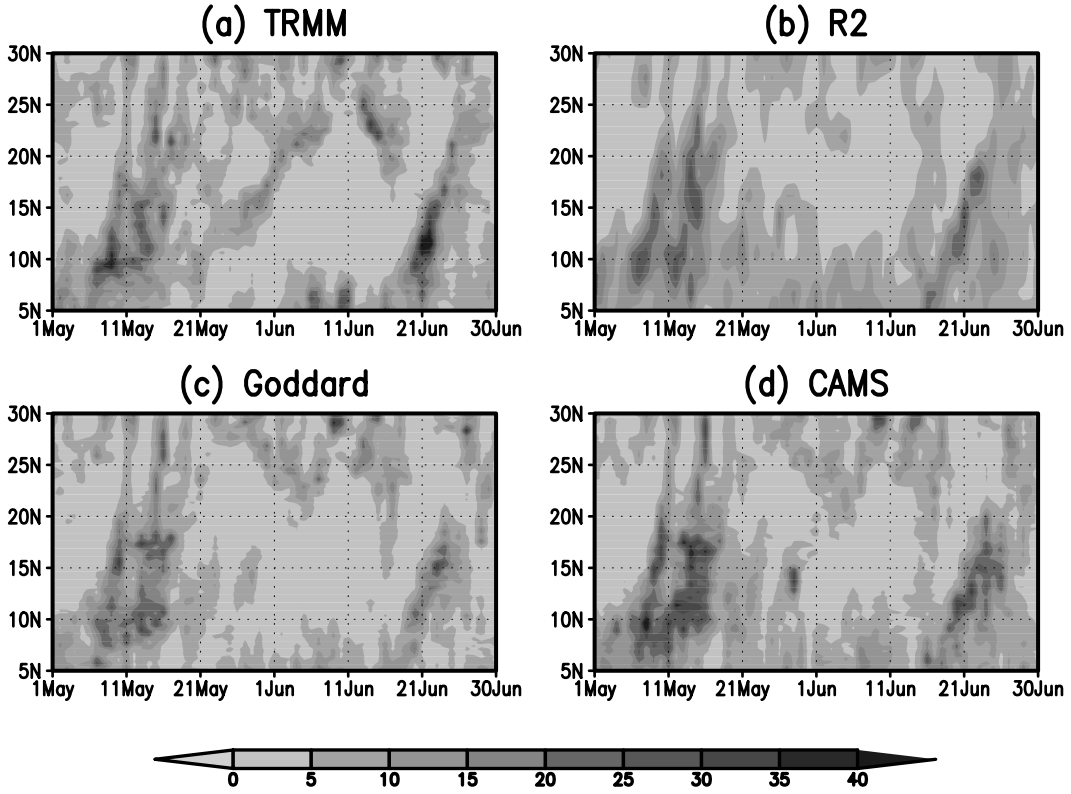

Fig. 5. Precipitation (mm d^{-1}) as a function of time and latitude averaged over 110°–145°E from (a) TRMM, (b) R2, and (c, d) WRF simulations.

along the longitudinal band between 110°E and 145°E. Two major phases (middle of May and end of June) of northward movement of the convection zone from near the equator to about 25°N can be seen. The average speed of northward propagation was about 1.0° latitude per day. The northward movement reflected the seasonal migration of the EA–WNP monsoon rain bands. The WRF model and R2 reanalysis generally reproduced the two northward marches of rain bands. However, they both failed to simulate the weak northward rain band from 10°N to 25°N in the period from the end of May to early June. In addition, the temporal correlation coefficients between TRMM-observed and WRF-simulated daily precipitation were similar to those between TRMM-observed and R2 (averaged ∼0.34), indicating that the current WRF downscaling simulation does not improve the temporary variability significantly. This is due to there being many atmospheric variability fields, which leads to precipitation being constrained by observations twice a day in the reanalysis data, so no obvious improvement is achieved in the timing of precipitation.

4.3 *Precipitation frequency*

Next, we analyzed the frequency distributions of rainy days and precipitation amounts. The percentages of all days with precipitation exceeding 0.1 mm d^{-1} (the definition of a rainy day in this study) and 50 mm d^{-1} during May to June 2008 were calculated. The percentage of rainy days can often be affected by the use of re-gridded data (Osborn and Hulme, 1997; Ensor and Robeson, 2008), which potentially can generate systematic biases in any comparisons being made. For example, the averaged precipitation frequency of rainy days will increase by around 15% when using re-gridded data instead of original data. Therefore, in this study, the results from all original model outputs were used when calculating the precipitation frequency.

The percentage of rainy days according to the TRMM dataset is higher over the southernmost and northernmost regions of domain 3. The R2 data overestimate the frequency of rainy days over the ocean compared to the TRMM dataset. As we expected, the patterns of rainy day frequency improved in the WRF simulations compared to R2-based results (Fig. 6). The WRF simulations evidently reduced the percentage of rainy days in the southern part of the domain and increased that in the northern part, conforming to the TRMM observations. Note that the CAMS two-moment scheme produced a few more rainy days than the Goddard one-moment scheme (areas where

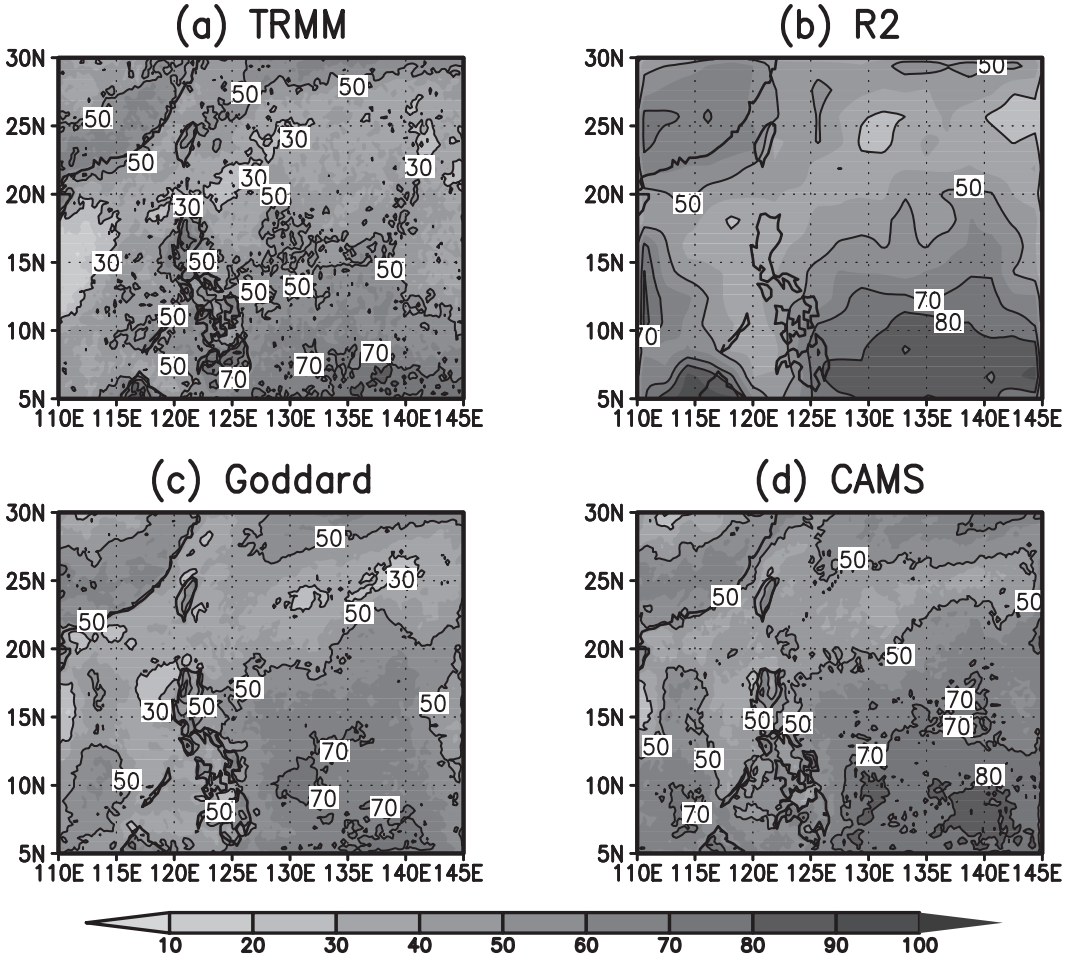

Fig. 6. Percentage of days with precipitation rate exceeding 0.1 mm d^{-1} during May to June 2008 from (a) TRMM, (b) R2, and (c, d) WRF simulations.

the percentage of rainy days was less than 30% were found). This is consistent with the conclusion of Morrison et al. (2009), who found that the two-moment microphysics scheme can produce a wider spread of stratiform precipitation as a result of a weaker rain evaporation rate below the melting layer, compared to the one-moment microphysics in the stratiform region. The rate of rain evaporation is related to the raindrop intercept parameter, which is specified as a fixed value in the Goddard one-moment scheme (8×10^6 m^{-4}) and is usually larger than that in the CAMS two-moment scheme in the stratiform region. That is, the raindrop number concentration in the CAMS scheme is less than that in the Goddard scheme in the stratiform region, resulting in a weaker rain evaporation rate and, subsequently, a greater frequency of rainy days. Additionally, the representation of droplet number concentration is another probable reason for the difference (no droplet number concentration in the Goddard scheme). Saleeby et al. (2010) showed an increase in aerosol concentration over the East China Sea by the discrepancies in rainfall estimates between the TRMM PR and TMI sensors. The droplet number concentration from the CAMS scheme (sometimes up to 3×10^8 m^{-3}) is like the real environment, and will reduce the autoconversion efficiency of cloud water to rain under the same atmospheric conditions, especially relative humidity. As a result, the raindrop number concentration decreases and the raindrop mean diameter increases, leading to high rainfall frequency during the precipitation formation process in the case of sufficient water vapor.

Table 2 shows the mean precipitation amount, percentage of rainy days, and precipitation intensity (precipitation divided by percentage of rainy days) averaged over domain 3. Some previous studies have focused on these characteristics of precipitation (Dai, 2001; Sun et al., 2006). The percentage of rainy days

Table 2. Area-averaged daily mean precipitation (mm d^{-1}), percentage of rainy days (%) and precipitation intensity (mm d^{-1}).

	Mean	Rainy days	Intensity
TRMM	7.03	47.4	14.8
R2	7.38	55.6	13.3
Goddard	6.24	49.1	12.7
CAMS	8.01	57.1	14.0

with precipitation exceeding 0.1 mm d^{-1} from the TRMM dataset was 47.4%. The R2 data and the WRF model outputs fell between 49.1% and 57.1%, slightly larger compared to the results from the TRMM observations. The percentage of rainy days from the Goddard scheme tends to be lower than that from the CAMS scheme, as discussed above. As a result, the model precipitation intensities from R2 data and WRF simulations were slightly weaker than the TRMM precipitation intensity.

The percentage of days with heavy precipitation (exceeding 50 mm d^{-1}) is shown in Fig. 7. Typical summer monsoon heavy rainbands are located over the Philippine Sea, SCS, and southeast China coast. The R2 results, limited by the coarse resolution and cumulus parameterization, showed an underestimation of heavy rainfall events compared to the TRMM observations. The WRF downscaling simulations evidently improved upon the R2-based results, especially over southeastern China and SCS. However, the CAMS scheme overestimated the frequency of heavy precipitation by up to 3–6 percentage points over the Philippine Sea, resulting in larger precipitation amounts over that region. Note that the broad feature of heavy precipitation frequency followed a similar spatial pattern to that of daily mean precipitation (Fig. 4), especially for the locations with maximum values. This indicates that the maximum accumulated precipitation amount is clearly attributable to the heavy precipitation events.

To further examine the rainfall frequency distribution, the observed TRMM daily precipitation in the period May to June 2008 within domain 3 was partitioned into 12 bins (only rainy days were included),

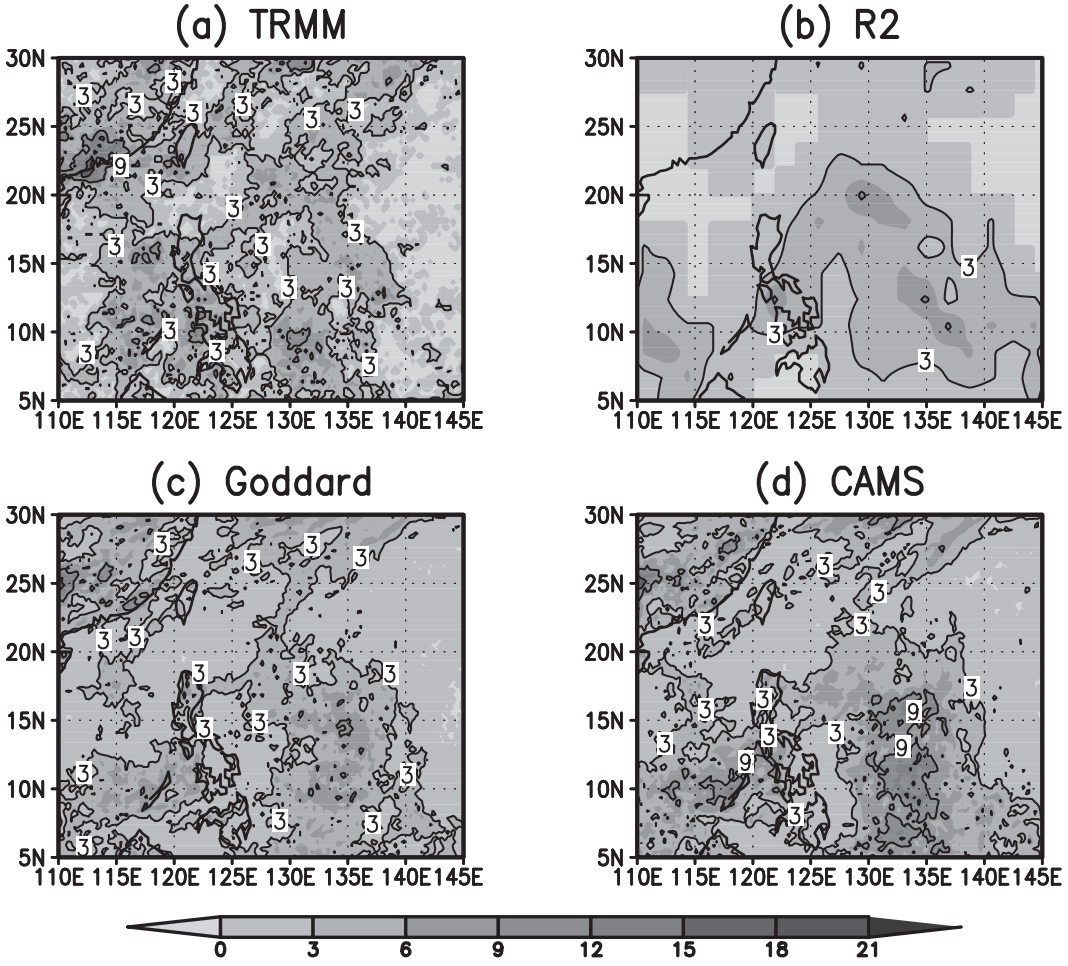

Fig. 7. The same as Fig. 6, but for precipitation rate exceeding 50 mm d^{-1}.

covering the first nine decile bins (0%–10%, 10%–20%, ... 80%–90%) and the 90%–95%, 95%–99%, and 99%–100% bins. In the following discussion, the 0%–30% bin is taken as light precipitation, the 30%–60% bin as moderate precipitation, the 60%–90% bin as heavy precipitation, the 90%–100% bin as very heavy precipitation, and the top 1% as extreme precipitation.

In addition to the TRMM data, we also calculated R2-based frequency distributions and WRF-simulated rainfall data. The results are shown in Fig. 8. For light precipitation, and in the first percentile bin in particular (precipitation rates between 0.1 and 0.6 mm d^{-1}), the WRF-simulated frequency was much higher, while that based on R2 data was lower. Some previous studies have also reported an overestimation of light precipitation by the Goddard microphysics scheme in a 3-month simulation (Liu et al., 2011). For moderate to heavy precipitation, the WRF-simulated frequency was generally lower, whereas that from R2 data was somewhat higher. Moreover, R2 obviously underestimated very heavy precipitation, especially the top 1% extreme precipitation (>107.5 mm d^{-1}). The above features confirm the reasoning that R2 cannot resolve the physical processes associated with intense mesoscale weather systems to produce extreme precipitation. The WRF model was found to overestimate the rainfall distributions of small events at the expense of large ones and slightly overestimate extreme events at the expense of small ones, resulting in less moderate to heavy precipitation. The WRF-simulated extreme events were in good agreement with the TRMM observations because of the cloud-resolving microphysics within the high-resolution WRF model. A better representation of climate extremes is a key consideration for regional climate simulation, and the WRF results reported here show reasonable skill and add more value to the downscaling approach in reproducing very heavy precipitation.

The WRF-simulated precipitation frequency by the two cloud schemes in Fig. 8 show that the CAMS scheme produced less frequent light rains and slightly more frequent heavy rains compared with those from the Goddard scheme. Note that only the days with precipitation amount exceeding 0.1 mm d^{-1} were used in the statistics. Li et al. (2011) showed that light rains occur less frequently and heavy rains occur more frequently under polluted conditions compared to clean conditions using observations from a site on the Southern Great Plains during summer seasons. Here, the simulated droplet concentration in the CAMS scheme sometimes reached up to $\sim 3\times10^8$ m^{-3} and was higher than the common value over the ocean ($\sim 0.5\times10^8$ m^{-3}), to a certain extent like the real polluted conditions over the WNP region (Berg et al., 2008). In addition, the features of precipitation frequency distribution from R2 were qualitatively opposite to those from WRF simulations, probably due to the different moisture physics treatment, i.e., the cloud-resolving microphysics used in the WRF model versus the cumulus parameterization used in R2. The stratiform precipitation area simulated by cloud-resolving microphysics is usually larger than that by cumulus parameterization (Chin et al., 2010).

To investigate the distribution of precipitation

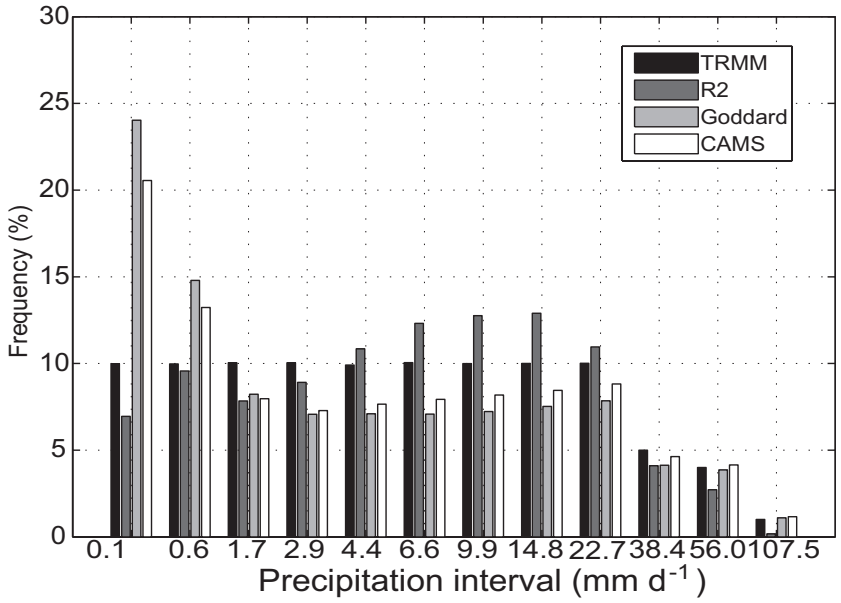

Fig. 8. Probability distribution of observed and simulated daily precipitation at different intervals over domain 3.

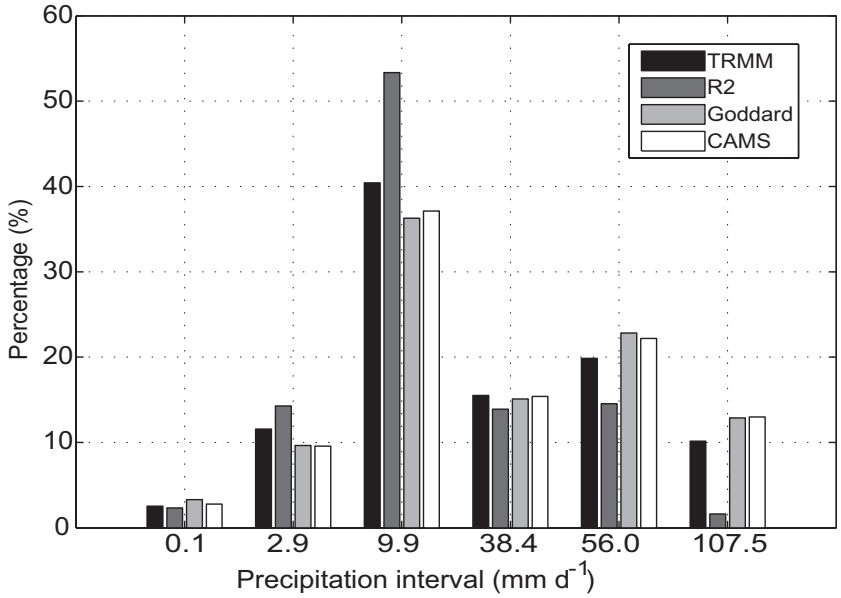

Fig. 9. Percentage of observed and simulated precipitation amount as a function of precipitation rate over domain 3.

amount, Fig. 9 shows the observed and simulated percentage of precipitation amount in the two summer monsoon months over domain 3 as a function of precipitation rate. The bins used here represent light (0–30%), moderate (30%–60%), heavy (60%–90%), and very heavy (90%–95%, 95%–99% and 99%–100%) precipitation, respectively. The TRMM observations exhibited a broad frequency distribution with the peak between 9.9 and 38.4 mm d^{-1} (the third bin, heavy rain). The WRF simulations produced slightly more light precipitation than the TRMM observations because of too many light rain days (Fig. 8). Light precipitation contributed only about 3% of the total precipitation amount, although the occurrence frequency was the highest. The total precipitation amount came mainly from the heavy precipitation bin, and R2 overestimated the contribution of heavy precipitation to total precipitation (∼53%) because of the higher occurrence frequency. In addition, the percentages for very heavy precipitation (exceeding 56 mm d^{-1} above top 5%) in R2 decreased rapidly, corresponding to the lower occurrence frequency of very heavy precipitation. On the contrary, the WRF simulations were slightly stronger, but close to the TRMM observations. The accumulated extreme precipitation amount (top 1%) was comparable to that of moderate precipitation (second bin).

One of the main advantages of dynamical downscaling identified in previous studies is the improvement in simulating extreme events over land due to a more realistic representation of topography. Our results also showed a notable improvement in simulated extreme precipitation over the ocean, apparently due to explicitly resolved cloud microphysics with high spatial resolution. Note that some heavy precipitation events over the southeast China coast were included in our analysis, but the majority of very heavy precipitation events occurred over the WNP region, and the rainfall statistics shown in Figs. 8 and 9 were not affected.

5. Hydrologic budgets

In this section, the hydrologic budget is analyzed to further understand relevant precipitation processes. We calculated the atmospheric hydrologic budget averaged over domain 3 during May to June 2008 by the following conservations equation for water vapor (Peixoto and Oort, 1983):

$$\frac{\partial}{\partial t}\frac{1}{g}\int_{p_s}^{0} q\,dp + \nabla\cdot\frac{1}{g}\int_{p_s}^{0} q\boldsymbol{V}\,dp = E - P\,, \qquad (1)$$

where q and $\boldsymbol{V}$ are specific humidity and horizontal wind vector at pressure level p, respectively; p_s is the surface pressure; the first two terms on the left-hand side represent the tendency change of precipitable water and the moisture flux divergence, respectively; and E and P on the right-hand side are surface evaporation and precipitation, respectively. We used the 6-hourly reanalysis data and model outputs to calculate the above budget terms.

Figure 10 shows the simulated daily mean moisture convergence, evaporation, precipitable water tendency,

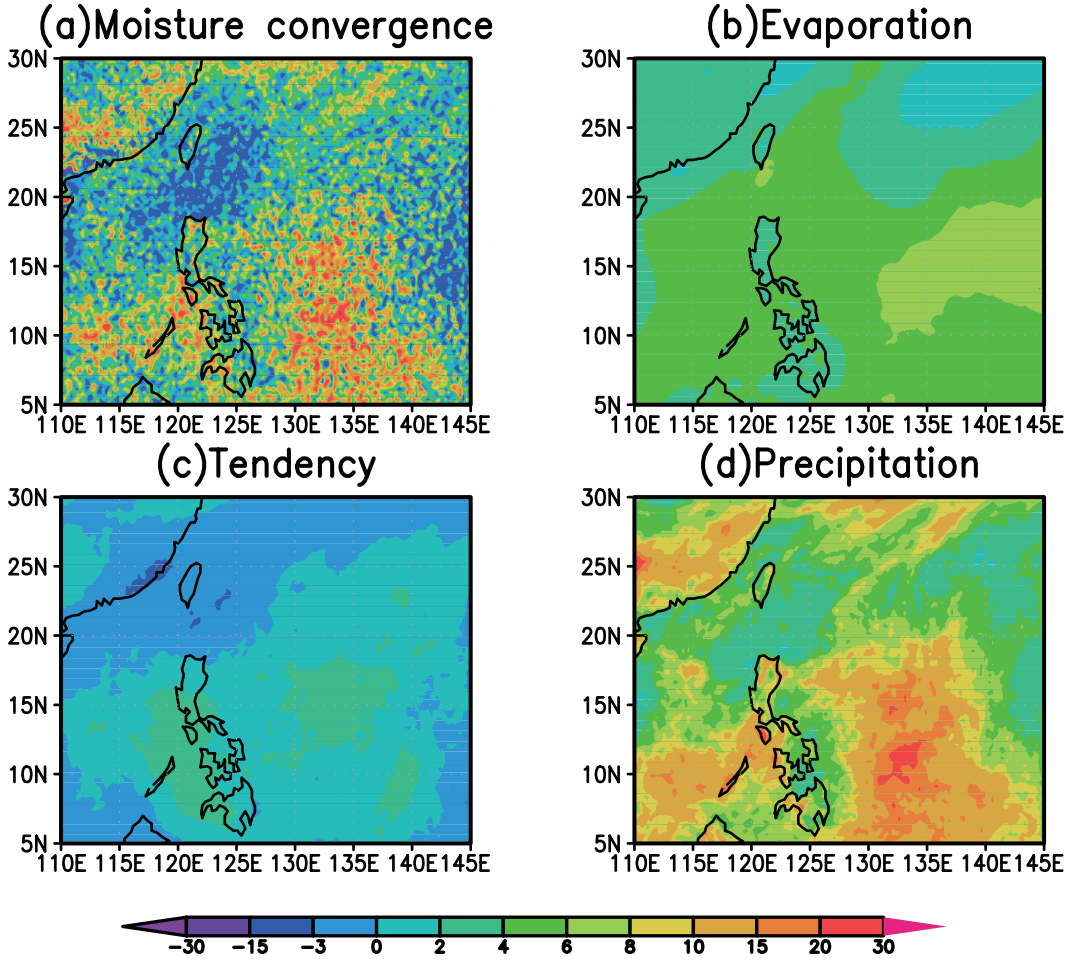

Fig. 10. Daily mean (a) moisture convergence, (b) evaporation, (c) precipitable water tendency, and (d) precipitation (mm d^{-1}) derived from the CAMS microphysics scheme during May to June 2008.

and precipitation by WRF with the CAMS scheme. The results show that the spatial distribution of precipitation coincided with that of moisture convergence, and evaporation had a near uniform distribution with a magnitude close to half of the precipitation amount. This is similar to the result of Xue et al. (2004) who argued that the monsoon precipitation over East Asia and West Africa is more closely related to the moisture convergence field than to surface evaporation.

Integration of Eq. (1) over domain 3 yields

$$\mathrm{MC} = P - E + dW \, . \tag{2}$$

Equation (2) states the total amount of water vapor that enters the domain (MC) should be balanced with the precipitation and precipitable water tendency (dW) minus evaporation (Wang and Yang, 2008). Figure 11 exhibits the time evolutions of the four moisture budget terms in Eq. (2) based on R2 data and WRF simulations. The red line denotes the residual term ($\mathrm{MC_{res}}$) defined as the sum of the three terms on the right-hand side of Eq. (2). The results show that the water vapor convergence in R2 forcing fields differed somewhat from the residual term $\mathrm{MC_{res}}$ (Fig. 11a). This imbalanced water vapor budget in reanalysis data is mainly induced by the artificial nudging process (Roads et al., 2002), but the imbalance from R2 here was small because the budget was averaged mostly over the ocean instead of over land (the latter being made up of mountains, various vegetation types etc., which can cause large differences in surface heating). The calculated budgets from the two WRF outputs were balanced with the vapor convergence (MC) in close agreement with $\mathrm{MC_{res}}$ (Figs. 11b and c). The temporal mean vapor budget terms in Eq. (2) for the period of May to June 2008 (Table 3) show that R2-based and WRF-simulated values of evaporation were basically similar (nearly 4 mm d^{-1}); however, the moisture convergence in the CAMS scheme was about three times stronger than that in the Goddard scheme. Consequently, the simulated total precipitat-

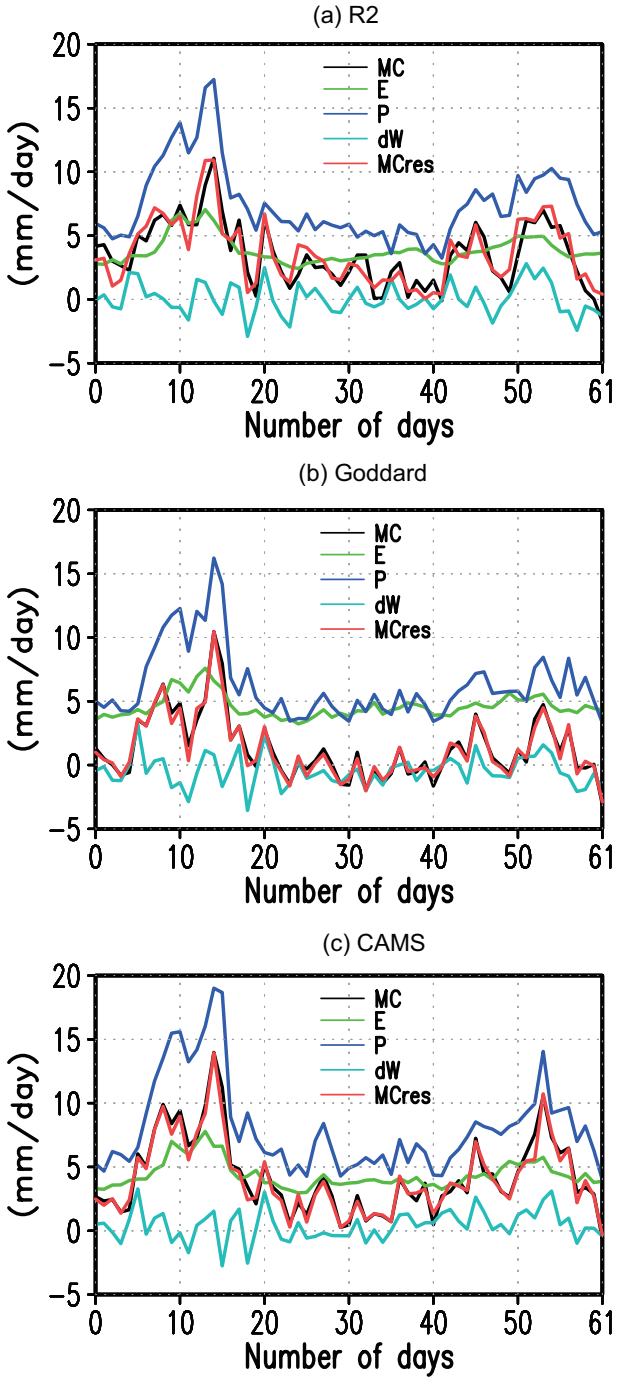

Fig. 11. Time evolution of the daily mean moisture budget averaged over domain 3 from (a) R2, (b) Goddard, and (c) CAMS simulations.

ion in the CAMS scheme was larger than that in the Goddard scheme. This is more evident in Fig. 11 during the periods of heavy precipitation in the middle of May and at the end of June; the precipitation intensity was quite consistent with the amount of moisture convergence, corresponding to the strong monsoon rain bands reported in Fig. 5. This indicates that the heavy precipitation events were contributed to mainly by the stronger moisture convergence. During less convective periods, the mean evaporation contributed more to the mean precipitation amount than the moisture convergence. The magnitude of mean precipitation with the Goddard scheme during these periods was almost the same as that of evaporation.

Table 3. The daily mean hydrologic budget terms (mm d^{-1}) averaged over domain 3 during May to June 2008.

	MC	E	P	dW
R2	3.03	3.86	7.38	0.05
Goddard	1.31	4.58	6.24	−0.45
CAMS	4.26	4.38	8.01	0.42

Figure 12 shows the mean moisture flux vector (m kg s^{-1} kg^{-1}) at 850 hPa and the corresponding moisture flux convergence fields (mm d^{-1}) averaged over May and June 2008 derived from R2 data and WRF simulations. The patterns of moisture flux convergence were generally in agreement with that of daily mean precipitation (Fig. 4), implying that the spatial distribution of precipitation is mainly decided by the moisture convergence field. Two major flows of water vapor transport are evident in the region of analysis: one from the Bay of Bengal, entering into southeastern China and the subtropical WNP region through the SCS; and the other from the tropical western Pacific, entering the subtropics along the western edge of the WNP subtropical high. The wind direction near the southern boundary in the Goddard scheme (Fig. 12b) was almost easterly, resulting in less water vapor transport into the domain. The moisture convergence from the CAMS scheme over the WNP region was stronger than that from the Goddard scheme because of the differences in simulated wind fields. In addition, the WRF simulations showed weaker moisture convergence over the western SCS and stronger moisture convergence over southeastern China compared to those in R2.

Although the two WRF simulations were subject to the same boundary forcing from R2, the two microphysics schemes caused considerable differences in the simulated location and strength of precipitation and atmospheric latent heating, which could further modify the large-scale circulation via thermodynamic feedback processes. The downscaling results suggest the importance of convective heating in summer monsoon climate over the WNP region. This is consistent with the tropical wave dynamics that latent heat release is a dominant forcing that drives the large-scale circulation (Chang et al., 1982). Therefore, a proper

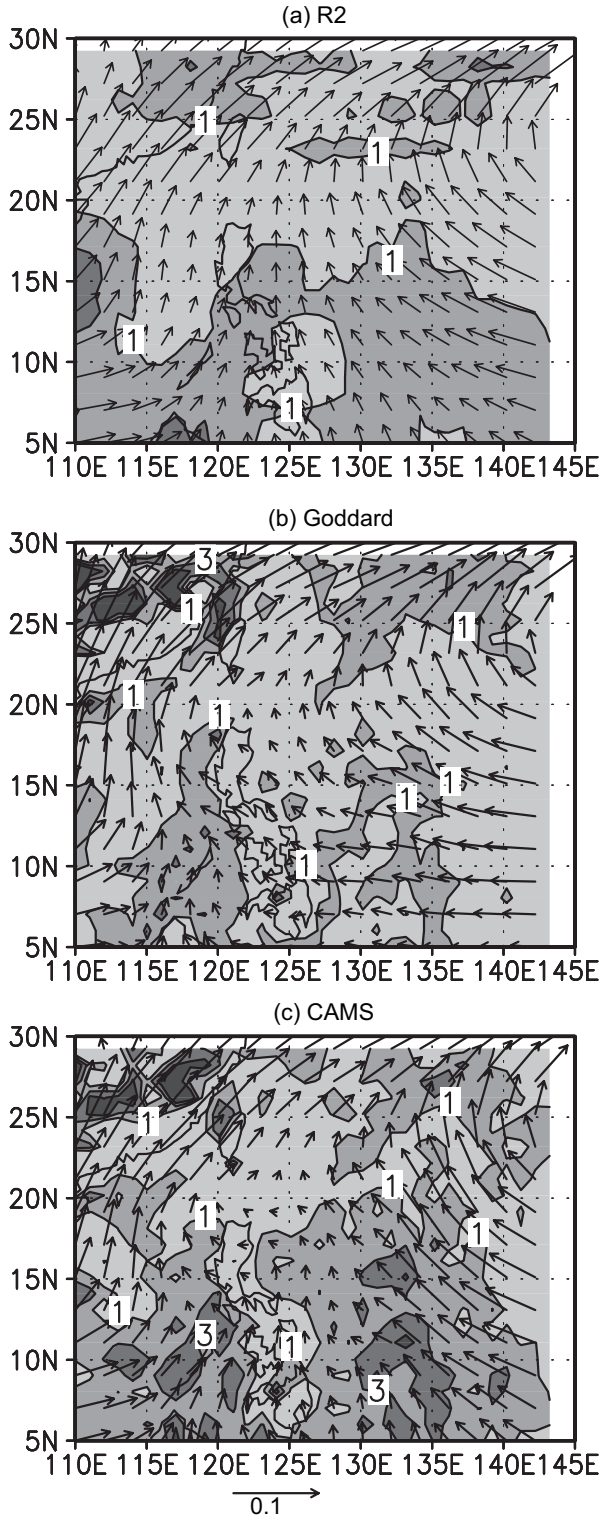

Fig. 12. Mean 850-hPa moisture flux vector (m kg s^{-1} kg^{-1}) with associated moisture convergence fields (mm d^{-1}) averaged over May and June 2008 from (a) R2, (b) Goddard, and (c) CAMS simulations.

representation of model microphysics is critical in simulating rainfall distribution and latent heating, which is as important as the large-scale dynamics governing tropical waves, monsoon surges, and climate oscillations in the tropical and WNP climate region.

6. Summary and conclusion

Precipitation is a key climate quantity, and reducing the precipitation bias is one of the major goals for improving climate simulations. In the work reported in this paper, we evaluated the capability of the cloud-resolving WRF model via a dynamical downscaling approach, in simulating regional precipitation, especially extreme precipitation events and the regional hydrologic budgets over the WNP region. The period of study was from May to June 2008, which is the period of transition from the onset of SCS monsoon to the WNP summer monsoon.

Our analysis indicates that R2 data represents the large-scale characteristics of daily mean precipitation over the WNP region well, but not the spatial distribution of extreme rainfall events. This is due to the low resolution and parameterized convective processes in R2, which inadequately resolve mesoscale precipitation features and smooth out the extreme events. The WRF downscaling simulations, however, reasonably produced a more detailed spatial distribution of daily mean precipitation as reflected by higher pattern correlation coefficients and smaller pattern RMSE with the TRMM observations.

The percentages of rainy days (exceeding 0.1 mm d^{-1}) from WRF simulations were evidently improved compared to R2-based results. The CAMS scheme produced a few more rainy days than that from the Goddard scheme. This is attributed to the two-moment microphysics scheme causing widespread stratiform precipitation due to weaker evaporation of rainwater below the melting layer relative to the one-moment microphysics. Meanwhile, the spatial patterns of rainy days with precipitation exceeding 50 mm d^{-1} from WRF simulations were similar to the spatial patterns of daily mean precipitation, indicating that the maximum accumulated precipitation amount is mainly contributed to by heavy precipitation events. In addition, the WRF simulations overestimated the frequency of light precipitation, somewhat underestimated the frequency of moderate to heavy precipitation, but represented the frequency of very heavy precipitation well, as compared with the frequency distribution from TRMM data.

The moisture convergence from WRF simulations balanced with the sum of precipitation and precipitable water tendency minus evaporation. During

more convective periods, the precipitation amount was primarily contributed to by moisture convergence. In less convective periods, the precipitation amount was contributed to more greatly by evaporation. The WRF simulations with the two microphysics schemes produced different budget balances. Compared with the R2 budget, the moisture convergence was smaller in the Goddard scheme but larger in the CAMS scheme. The significant difference in simulated vapor budgets indicates the importance in the tropical monsoon region of resolving convection that affects the precipitation, atmospheric latent heating and, subsequently, the large-scale circulation.

Acknowledgements. The authors are grateful to all colleagues and students who contributed to this study, especially to Dr. Wei-Kuo TAO for his insightful discussions. The authors also thank the anonymous reviewers for their valuable comments on an earlier version of this paper. We acknowledge the infrastructure support by the National Taiwan University and the high performance computer center in the National Central University. W. H. GAO was supported by the National Basic Research Program of China (Grant No. 2013CB955804, 2011CB403401) and 2012 National abroad personnel science and technology project. C.-H. SUI was supported by the National Science Council (Grant No. 100-2745-M-002-003-ASP). The TRMM 3B42 data were obtained from the Goddard Earth Sciences Data and Information Services Center at http://mirador.gsfc.nasa.gov/cgi-bin/mirador/presentNavigation.pl?tree=project&project=TRMM.

REFERENCES

Berg, W., T. L'Ecuyer, and S. van den Heever, 2008: Evidence for the impact of aerosols on the onset and microphysical properties of rainfall from a combination of satellite observations and cloud resolving model simulations. *J. Geophys. Res.*, **113**, D14S23, doi: 10.1029/2007JD009649.

Castro, C. L., R. A. Sr Pielke, and G. Leoncini, 2005: Dynamical downscaling: Assessment of value retained and added using the regional atmospheric modeling system (RAMS). *J. Geophys. Res.*, **110**, D05108, doi: 10.1029/2004JD004721.

Chang, C. B., D. J. Perkey, and C. W. Kreitzberg, 1982: A numerical case study of the effects of latent heating on a developing wave cyclone. *J. Atmos. Sci.*, **39**, 1555–1570.

Chen, F., and J. Dudhia, 2001: Coupling an advanced land-surface/ hydrology model with the Penn State/NCAR MM5 modeling system. Part I: Model description and implementation. *Mon. Wea. Rev.*, **129**, 569–585.

Chin, H.-N. S., P. M. Caldwell, and D. C. Bader, 2010: Preliminary study of California wintertime model wet bias. *Mon. Wea. Rev.*, **138**, 3556–3571.

Christensen, O. B., J. H. Christensen, B. Machenhauer, and M. Botzet, 1998: Very high-resolution regional climate simulations over Scandinavia-Present climate. *J. Climate*, **11**, 3204–3229.

Conroy, J. L., and J. T. Overpeck, 2011: Regionalization of present-day precipitation in the greater monsoon region of Asia. *J. Climate*, **24**, 4073–4095.

Dai, A., 2001: Global precipitation and thunderstorm frequencies. Part I: Seasonal and interannual variations. *J. Climate*, **14**, 1092–1111.

Dickinson, R. E., R. M. Errico, F. Giorgi, and G. T. Bates, 1989: A regional climate model for the western United States. *Climate Change*, **15**, 383–422.

Ding, Y. H., and D. R. Sikka, 2006: Synoptic systems and weather. *The Asian Monsoon*, Wang, Ed., Praxis Publishing Ltd., Chichester, 131–202.

Dudhia, J., 1989: Numerical study of convection observed during the winter monsoon experiment using a mesoscale two-dimensional model. *J. Atmos. Sci.*, **46**, 3077–3107.

Ensor, A. L., and S. M. Robeson, 2008: Statistical characteristics of daily precipitation: comparisons of gridded and point datasets. *J. Appl. Meteor. Climatol.*, **47**, 2468–2476.

Gao, W. H., F. S. Zhao, Z. J. Hu, and X. Feng, 2011a: A two-moment bulk microphysics scheme coupled with a mesoscale model WRF: Model description and first results. *Adv. Atmos. Sci.*, **28**, 1184–1200, doi: 10.1007/s00376-010-0087-z.

Gao, W. H., C.-H. Sui, T.-C. Chen Wang, and W.-Y. Chang, 2011b: An evaluation and improvement of microphysical parameterization from a two-moment cloud microphysics scheme and SoWMEX/TiMREX observations. *J. Geophys. Res.*, **116**, D19101, doi: 10.1029/2011JD015718.

Giorgi, F., 1990: Simulation of regional climate using a limited area model nested in a general circulation model. *J. Climate,* **3**, 941–963.

Giorgi, F., 2006: Regional climate modeling: Status and perspectives. *J. Phys. IV France*, **139**, 101–118.

Grell, G. A., and D. Devenyi, 2002: A generalized approach to parameterizing convection combining ensemble and data assimilation techniques. *Geophys. Res. Lett.*, **29**(14), 1693, doi: 10.1029/2002GL015311.

Hill, K. J., A. S. Taschetto, and M. H. England, 2011: Sensitivity of South American summer rainfall to tropical Pacific Ocean SST anomalies. *Geophys. Res. Lett.*, **38**, L01701, doi: 10.1029/2010GL045571.

Hong, S.-Y., and Y. Noh, and J. Dudhia, 2006: A new vertical diffusion package with an explicit treatment of entrainment processes. *Mon. Wea. Rev.*, **134**, 2318–2341.

Hu, Z. J., and G. He, 1988: Numerical simulation of microphysical processes in cumulonimbus, part 1: Microphysical model. *Acta Meteorologica Sinica*, **2**(4), 471–489.

Hu, Z. J., and G. He, 1989: Numerical simulation of microphysical processes in cumulonimbus, part 2: Case studies of shower, hailstorm and torrential rain. *Acta Meteorologica Sinica*, **3**(2), 185–199.

Huffman, G. J., R. F. Adler, D. T. Bolvin, G. Gu, E. J. Nelkin, K. P. Bowman, E. F. Stocker, and D. B. Wolff, 2007: The TRMM multisatellite precipitation analysis (TMPA): Quasi-global, multiyear, combined-sensor precipitation estimates at fine scale. *Journal of Hydrometeorology*, **8**, 38–55.

Jankov, I., J.-W. Bao, P. J. Neiman, P. J. Schultz, H.-L. Yuan, and A. B. White, 2009: Evaluation and comparison of microphysical algorithms in ARW-WRF model simulations of atmospheric river events affecting the California coast. *Journal of Hydrometeorology*, **10**, 847–870.

Jenkins, G. S., 1997: The 1988 and 1990 summer season simulations for West Africa using a regional climate model. *J. Climate*, **10**, 1255–1272.

Kanamitsu, M., and H. Kanamaru, 2007: Fifty-seven-year California reanalysis downscaling at 10 km (CaRD10). Part I: System detail and validation with observations. *J. Climate*, **20**, 5553–5571.

Kanamitsu, M., W. Ebisuzaki, J. Woollen, S.- K. Yang, J. J. Hnilo, M. Fiorino, and G. L. Potter, 2002: NCEP-DOE AMIP-II Reanalysis (R-2). *Bull. Amer. Meteor. Soc.,* **83**, 1631–1643.

Kobayashi, C., and M. Sugi, 2004: Impact of horizontal resolution on the simulation of the Asian summer monsoon and tropical cyclones in the JMA global model. *Climate Dyn.*, **93**, 165–176.

Kunkel, K. E., K Andsager, X. Z. Liang, R. W. Arritt, E. S. Takle, W. J. Jr Gutowski, Z. Pan, 2002: Observations and regional climate model simulations of heavy precipitation events and seasonal anomalies: a comparison. *Journal of Hydrometeorology,* **3**, 322–334.

Lau, K. M., and H. Y. Weng, 2002: Recurrent teleconnection patterns linking summertime precipitation variability over East Asia and North America. *J. Meteor. Soc. Japan,* **80**, 1309–1324.

Lee, D.-K., D.-H. Cha, and H.-S. Kang, 2004: Regional climate simulation of the 1998 summer flood over East Asia. *J. Meteor. Soc. Japan*, **82**, 1735–1753.

Leung, L. R., and Y. Qian, 2003: The sensitivity of precipitation and snowpack simulations to model resolution via nesting in regions of complex terrain. *Journal of Hydrometeorology*, **4**, 1025–1043.

Leung, L. R., L. O. Mearns, F. Giorgi, and R. L. Wilby, 2003: Regional climate research. *Bull. Amer. Meteor. Soc.*, **84**, 89–95.

Li, G., Y. Wang, and R. Zhang, 2008: Implementation of a two-moment bulk microphysics scheme to the WRF model to investigate aerosol-cloud interaction. *J. Geophys. Res.*, **113**, D15211, doi: 10.1029/2007JD009361.

Li, Z., F. Niu, J. Fan, Y. Liu, D. Rosenfeld, and Y. Ding, 2011: Long-term impacts of aerosols on the vertical development of clouds and precipitation. *Nature Geoscience*, **4**, 888–894.

Liang, X. Z., L. Li, K. E. Kunkel, M. Ting, and J. X. L. Wang, 2004: Regional climate model simulation of U.S. precipitation during 1982–2002. Part I: Annual cycle. *J. Climate*, **17**, 3510–3529.

Liu, C., K. Ikeda, G. Thompson, R. Rasmussen and J. Dudhia, 2011: High-resolution simulations of wintertime precipitation in the Colorado headwaters region: Sensitivity to physics parameterizations. *Mon. Wea. Rev.*, **139**, 3533–3553.

Lou, X., Z. Hu, Y. Shi, P. Wang, and X. Zhou, 2003: Numerical simulations of a heavy rainfall case in south China. *Adv. Atmos. Sci.*, **20**(1), 128–138.

Milbrandt, J. A., M. K. Yau, J. Mailhot, S. Bélair, and R. McTaggart-Cowan, 2010: Simulation of an orographic precipitation event during IMPROVE-2. Part II: Sensitivity to the number of moments in the bulk microphysics scheme. *Mon. Wea. Rev.*, **138**, 625–642.

Miura, H., M. Satoh, T. Nasuno, A. T. Noda, and K. Oouchi, 2007: A Madden-Julian oscillation event simulated by a global cloud-resolving model. *Science*, **318**, 1763–1765, doi: 10.1126/science.1148443.

Mlawer, E. J., S. J. Taubman, P. D. Brown, M. J. Iacono, and S. A. Clough, 1997: Radiative transfer for inhomogeneous atmosphere: RRTM, a validated correlated-k model for the longwave. *J. Geophys. Res.*, **102**, D14, 16663–16682.

Morrison, H., G.. Thompson, and V. Tatarskii, 2009: Impact of cloud microphysics on the development of trailing stratiform precipitation in a simulated squall line: Comparison of one- and two-moment schemes. *Mon. Wea. Rev.*, **137**, 991–1007.

Murakami, T., and J. Matsumoto, 1994: Summer monsoon over the Asian continent and western north Pacific. *J. Meteor. Soc. Japan*, **72**, 719–745.

Osborn, T. J., and M. Hulme, 1997: Development of a relationship between station and grid-box rainday frequencies for climate model evaluation. *J. Climate*, **10**, 1885–1908.

Peixoto, J. P., and A. H. Oort, 1983: The atmospheric branch of the hydrological cycle and climate. *Variations in the Global Water Budget*, Street-Perrott et al., Eds., Springer Netherlands, 5–65.

Qian, J.-H., A. Seth, and S. Zebiak, 2003: Reinitialized versus continuous simulations for regional climate downscaling. *Mon. Wea. Rev.*, **131**, 2857–2874.

Randall, D. A., and Coauthors, 2007: Climate models and their evaluation. *Climate Change 2007: The Physical Science Basis*, Solomon et al., Ed., Cambridge Univ. Press, New York, 589–662.

Roads, J., M. Kanamitsu, and R. Stewart, 2002: CSE water and energy budgets in the NCEP-DOE reanalysis II. *Journal of Hydrometeorology,* **3**, 227–248.

Saleeby, S. M., W. Berg, S. van den Heever, and T. L'Ecuyer, 2010: Impact of cloud-nucleating aerosols in cloud-resolving model simulations of warm-rain precipitation in the East China Sea. *J. Atmos. Sci.*, **67**, 3916–3930.

Satoh, M., T. Inoue, and H. Miura, 2010: Evaluations of cloud properties of global and local cloud system resolving models using CALIPSO and CloudSat simulators. *J. Geophys. Res.*, **115**, D00H14, doi: 10.1029/2009JD012247.

Skamarock, W. C., J. B. Klemp, J. Dudhia, D. O. Gill, D. M. Barker, W. Wang, and J. G. Powers, 2008: A description of the advanced research WRF version 3. NCAR Technical Note, NCAR/TN-475+STR, 123pp. [Available online at http://www.mmm.ucar.edu/wrf/users/docs/arw_v3.pdf.]

Sun, Y., S. Solomon, A. Dai, and R. Portmann, 2006: How often does it rain? *J. Climate*, **19**, 916–934.

Tao, W.-K., and J. Simpson, 1993: The Goddard cumulus ensemble model. Part I: Model description. *Terrestrial, Atmospheric and Oceanic Sciences*, **4**, 35–72.

Tao, W.-K., and Coauthors, 2003a: Microphysics, radiation and surface processes in the Goddard Cumulus Ensemble (GCE) model. *Meteor. Atmos. Phys.*, **82**, 97–137.

Tao, W.-K., Y. Wang, J.-H. Qian, C.-L. Shie, K.-M. Lau, and R. Kakar, 2003b: Mesoscale convective systems during SCSMEX: Simulations with a regional climate model and a cloud-resolving model. Weather and Climate Modeling: *INDO-U.S. Climate Research Program*, Singh et al., Eds., New Age International, 77–92.

Wang, B., and LinHo, 2002: Rainy season of the Asian-Pacific summer monsoon. *J. Climate*, **15**, 386–398.

Wang, B., and H. Yang, 2008: Hydrological issues in lateral boundary conditions for regional climate modeling: Simulation of East Asian summer monsoon in 1998. *Climate Dyn.*, **31**, 477–490.

Wang, B., R. Wu, and K.-M. Lau, 2001: Interannual variability of the Asian summer monsoon: Contrasts between the Indian and the western North Pacific-East Asian monsoons. *J. Climate*, **14**, 4073–4090.

Wang, Y., O. L. Sen, and B. Wang, 2003: A highly resolved regional climate model (IPRC-RegCM) and its simulation of the 1998 severe precipitation event over China: I. Model description and verification of simulation. *J. Climate*, **16**, 1721–1783.

Weisman, M. L., W. C. Skamarock, and J. B. Klemp, 1997: The resolution dependence of explicitly modeled convective systems. *Mon. Wea. Rev.*, **125**, 527–548.

Winterfeldt, J., B. Geyer, and R. Weisse, 2010: Using QuikSCAT in the added value assessment of dynamically downscaled wind speed. *Int. J. Climatol.*, **31**, 1028–1039, doi: 10.1002/joc.2105.

Wu, B., T. J. Zhou, and T. Li, 2009: Contrast of rainfall-SST relationships in the western North Pacific between the ENSO-developing and ENSO-decaying summers. *J. Climate*, **22**, 4398–4405.

Xue, Y., H.-M. H. Juang, W.-P. Li, S. Prince, R. DeFries, Y. Jiao, and R. Vasic, 2004: Role of land surface processes in monsoon development: East Asia and West Africa. *J. Geophys. Res.*, 109, D03105, doi: 10.1029/2003JD003556.

Zhou, T. J., and R. C. Yu, 2005: Atmospheric water vapor transport associated with typical anomalous summer rainfall patterns in China. *J. Geophys. Res.,* **110**, D08104, doi: 10.1029/2004JD005413.

Zhou, T. J., and Coauthors, 2009: The CLIVAR C20C project: Which components of the Asian–Australian monsoon circulation variations are forced and reproducible? *Climate Dyn.*, **33**, 1051–1068.